Electrochimica Acta 424 (2022) 140649

Contents lists available at ScienceDirect

Electrochimica Acta

journal homepage: www.journals.elsevier.com/electrochimica-acta

High frequency response of adenine-derived carbon in aqueous electrochemical capacitor

Justyna Piwek [a], Adam Slesinski [a,$,*], Krzysztof Fic [a], Sergio Aina [b], Alen Vizintin [c], Blaz Tratnik [c], Elena Tchernychova [c], Maria Pilar Lobera [b,d], Maria Bernechea [b,d,e], Robert Dominko [c,f,g], Elzbieta Frackowiak [a,#,*]

[a] Institute of Chemistry and Technical Electrochemistry, Poznan University of Technology, 60-965 Poznan, Poland
[b] Instituto de Nanociencia y Materiales de Aragón (INMA) CSIC-Universidad de Zaragoza, Department of Chemical and Environmental Engineering, University of Zaragoza, Campus Río Ebro-Edificio I+D, C/ Mariano Esquillor S/N, 50018 Zaragoza, Spain
[c] National Institute of Chemistry, Hajdrihova 19, 1000 Ljubljana, Slovenia
[d] Networking Research Center on Bioengineering, Biomaterials and Nanomedicine, CIBER-BBN, 28029 Madrid, Spain
[e] ARAID, Government of Aragon, 50018, Zaragoza, Spain
[f] Faculty of Chemistry and Chemical Technology, University of Ljubljana, Večna pot 113, 1000, Ljubljana, Slovenia
[g] ALISTORE-European Research Institute, CNRS FR 3104, Hub de l'Energie, Rue Baudelocque, 80039, Amiens Cedex, France

ARTICLE INFO

Keywords:
Electrode materials
Electrochemical capacitor
High-frequency response
N-rich carbon

ABSTRACT

Electrochemical capacitors are attractive power sources, especially when they are able to operate at high frequency (high current regime). In order to meet this requirement their constituents should be made of high conductivity materials with a suitable porosity. In this study, enhanced power and simultaneously high capacitance (120 F g^{-1} at 1 Hz or 10 A g^{-1}) electrode material obtained from carbonized adenine precursor is presented. A micro/mesoporous character of the carbon with optimal pore size ratio and high surface area was proven by the physicochemical characterization. The beneficial pore structure and morphology resembling highly conductive carbon black, together with a significant nitrogen content (5.5%) allow for high frequency response of aqueous capacitor to be obtained. The carbon/carbon symmetric capacitor (in 1 mol L^{-1} Li_2SO_4) has been tested to the voltage of 1.5 V. The cyclic voltammetry indicates a good electrochemical response even at high scan rate (50 mV s^{-1}). The cyclability of the capacitor is comparable to the one operating with commercial carbon (YP50F). The adenine-based capacitor is especially favourable for stationary applications requiring high power.

1. Introduction

Electrical double layer capacitors (EDLCs) known also as electrochemical capacitors (ECs) are very popular and widely developed energy storage systems which are characterized by high specific power and long cycle life [1–3]. The main role in EDLCs construction plays the activated carbon electrode and selected electrolyte [4–6]. Their operation principle is based on electrostatic attraction, where the ions from electrolyte are adsorbed on carbon surface forming the electric double layer. Therefore, it is imperative to use microporous carbons with a high specific surface area (1000–2000 m^2 g^{-1}) in order to obtain satisfactory specific capacitance values (ca. 100 F g^{-1} when calculate per electrode) [7–9]. Nevertheless, in order to ensure an effective ion fluxes during charging/discharging processes, mesopores presence is of high importance. They act as the transport channels for ions movement during EDL formation [10–12].

During the last years, many attempts of electrochemical capacitors (EC) metrics enhancement are carried out. One trend is to improve the operating voltage which in the case of aqueous electrolytes is limited due to the thermodynamic water decomposition at 1.23 V. Nevertheless, some research studies proved that for neutral pH alkali metal salt much higher voltage can be applied. Another option is to use organic medium,

* Corresponding authors.
E-mail addresses: adam.slesinski@put.poznan.pl (A. Slesinski), elzbieta.frackowiak@put.poznan.pl (E. Frackowiak).
$ ORCID: 0000–0001–9074–9645.
# ORCID: 0000–0003–2518–3950

https://doi.org/10.1016/j.electacta.2022.140649
Received 7 February 2022; Received in revised form 6 May 2022; Accepted 28 May 2022
Available online 29 May 2022

however, in comparison to aqueous electrolytes much lower power rates are obtained due to low conductivity values of non-aqueous solutions (e.g., 1 mol L^{-1} $Li_2SO_{4(aq)}$ – 60 mS cm^{-1} and 1 mol L^{-1} $TEABF_4$ in $AN_{(org)}$ 20 mS cm^{-1}) [2,13]. Additionally, oxygen and water free atmosphere and special carbon drying are required for organic medium what creates additional costs for ECs construction. The second approach for energy density improvement in ECs is capacitance increase. It can be realized by introduction of redox active species to the studied system. Some research shows the possibility of redox electrolyte application (e.g., iodides [14], bromides [15], thiocyanates [16]) but in addition carbon electrode can be enriched with oxygen or nitrogen surface functional groups [17,18]. Heteroatom doping of activated carbon (AC) has been studied for the last years demonstrating its advantage in supercapacitor performance. More precisely, N-doping was found to increase the capacitance of AC through faradaic reactions, improved conductivity and better wettability [19]. To prepare doped material, the source of desired element is required. O-rich carbons are obtained by their oxidation in air [20], HNO_3 [21] or electrochemical oxidation [22], while N-rich carbons can be realized *via* ammonia [23], urea, melamine or polyaniline chemical treatment [17,24]. Oxygen surface functionalities (e.g., quinone/hydroquinone [25]) may enhance carbon wettability and the capacitance values of EC system due to its pseudocapacitive character (especially in acidic medium [26]), however, usually at the expense of power density and cycle life. Besides, higher self-discharge rates are recorded for oxygen-rich carbons due to redox shuttle effects [27]. N-rich carbons are beneficial EC materials, however, nitrogen content should not exceed 8 wt.% [4]. Each type of N (pyrrolic, pyridinic, graphitic…) provides different benefits [18,28, 29]. Negatively charged pyrrolic and pyridinic N are placed at the edges of the carbon structure. They contribute to the pseudocapacitance due to their e-donor behaviour. They are able to donate p-electrons to the π-system of the aromatic rings [19,30]. On the other hand, quaternary nitrogen is placed into the basal plane substituting one carbon atom. The positive charge helps with the electron transfer through the material [18,31]. Additionally, oxygen functional groups have been studied as they can contribute to the capacitance of the material in aqueous electrolyte [32]. In fact, increase in capacitance has been attributed to the electron acceptor characteristics of quinone groups [33]. Moreover, hydroxyl groups might produce a charge bias that enhances the formation of the electric double-layer (EDL) in supercapacitors [34]. Carboxyl and hydroxyl polar groups are also associated with improved wettability of carbon materials [35,36]. The conductivity of chosen materials plays a crucial role when capacitor systems are considered. In those enhanced conditions, EDLC system is able to operate at high frequency (high current regime). Therefore, proper electrode functionalization may contribute to increased capacitance and improved EDLC overall performance. However, one should remember about proper amount of introduced species. To prepare hierarchical heteroatom carbons, there are many methods, such as, hard and soft templating methods [37,38] and ionothermal or so-called salt templating methods [39–41]. Salt templating method offers the possibility to tune the carbon synthesis to produce a micro- and mesoporous heteroatom doped carbon depending on the used inorganic template. Especially, the eutectic inorganic salt mixtures, such as $LiCl/ZnCl_2$, $NaCl/ZnCl_2$ or $KCl/ZnCl_2$ [42] give tuning opportunities.

In this paper, activated carbon based on nitrogen-rich adenine precursor for ECs application is demonstrated. To reach developed surface area of carbon a soft-templating synthesis method was used. The performance of two-electrode capacitor system (with 1 mol L^{-1} Li_2SO_4 electrolyte) is compared to the commercially available carbon Kuraray YP50F. It has been proven that superior gravimetric capacitance comparing to commercial carbon as well as the outstanding frequency response is obtained in ECs. The extensive studies including the electrochemical data connected with in-depth physicochemical analysis aims at verification of this advantageous effect.

2. Experimental

The experimental part is divided into sections containing the description of consecutive steps undertaken in the research.

2.1. Carbon synthesis

The AdeKZ carbon was obtained *via* salt template technique [40,41]. First, 53 g potassium chloride (Sigma Aldrich, 99%) and 97 g zinc chloride (Riedel de Haen, 98%) were freshly grinded, which results in a molar ratio of 1:1. Second, 150 g of salt mixture was mixed with 15 g of adenine (Alfa Aesar, 99%), which served as heteroatom doped carbon precursor. Salt to precursor weight ratio was 10:1. The mixture was placed into a ceramic crucible and it was carbonized in the quartz tubular furnace at 900 °C for 1 h in argon atmosphere. The heating and cooling rates were 2.5 °C/min. The obtained product was grinded and washed with 10% HCl followed by deionized water until neutral pH was reached. The purified AdeKZ was dried in a vacuum oven at 90 °C for 24 h.

2.2. Physicochemical characterization and microscopy

Physicochemical measurements include the Brunauer-Emmett-Teller (BET) specific surface area (S_{BET}) measurements determined by N_2 sorption at 77 K using porosity analyser ASAP 2460 (Micromeritics Instrument Corporation). First, the samples were degassed for 12 h in helium flow at 120 °C. Afterwards, they were outgassed in the vacuum for 5 h. The BET specific surface area value was determined in a relative pressure (p/p_0) range equal to 0.01–0.05. The pore size distribution was calculated by the algorithm of Saieus® software (Micromeritics Instrument Corporation) using 2D-NLDFT model. Particle size distribution was measured on Mastersizer 3000 (Malvern Panalytical).

The conductivity of the composite electrodes was measured using custom four-electrode measurement setup.

ζ-Potential measurements were done using a Brookhaven equipment. Both samples (AdeKZ and YP50F) were analysed 5 times in automatic mode when residual signal reached <0.003, the samples were suspended in a 1 mM KCl solution, pH = 5.6.

FTIR measurements were performed using Vertex-70 FTIR spectrophotometer (Bruker, USA). Data points were collected at a resolution of 4 cm^{-1} and 40 number of scans.

The determination of the mass fractions of carbon, hydrogen, nitrogen and oxygen was carried out in Thermo Scientific FlashSmart equipment. The oxygen amount was obtained via direct (separate) elemental analysis. The presented results in this paper are the average value from three separate analyses.

X-ray photoelectron spectroscopy (XPS) was performed with an Axis Supra spectrometer (Kratos Tech). The spectra were excited by a monochromatized Al Kα source at 1486.6 eV and subsequently run at 8 kV and 15 mA. A survey spectrum was measured at 160 eV of pass energy, and for the individual peak regions, spectra were recorded with a pass energy of 20 eV. Analysis of the peaks was performed with the CasaXPS software using a weighted sum of Lorentzian and Gaussian component curves after Shirley background subtraction. The binding energies were referenced to the internal C1s standard at 284.6 eV.

Scanning electron microscope (FE-SEM, Supra 35 VP Carl Zeiss) was used to characterize the morphology of the samples with in-lens detector at 1 kV electron high tension (EHT) voltage. Probe Cs-corrected scanning transmission electron microscope (STEM) JEM-ARM200CF equipped with a cold field emission (FEG) electron source operated at 80 kV and JEOL STEM detectors (JEOL, Tokyo, Japan), was employed to examine the materials morphology and particles' distribution.

TEM samples were prepared by dispersing approximately 200 μg of the material in 5 mL of absolute ethanol in an ultrasonic bath for 15 min. Then, 20 μL of the suspension was placed on the copper TEM grid. For the materials imaging, scanning high resolution high-angle annular

dark-field/bright-field (STEM-HAADF, STEM-BF) modes were used.

3. Electrochemical characterization

The activated carbon materials in the form of powder were turned into the composite electrode using PTFE binder. The activated carbon (AC) was mixed with conductive additive carbon black Super C65 (CB, Imerys) and aqueous polytetrafluoroethylene dispersion (Sigma-Aldrich) in isopropanol. The weight ratio of components was 90:5:5, respectively. The dispersion was thoroughly mixed and after that the isopropanol was evacuated using rotary vacuum evaporator. The resulting dry powdery material was enriched with small amount of isopropanol to form a continuous jelly structure which could be then rolled into a thin film electrode material. The final material was dried in a convective oven overnight at 80 °C for the complete isopropanol removal. The final thickness of the composite was 220 μm. The obtained carbon film was cut into the circular electrodes of 10 mm diameter. The weight of single electrode was dependant on the carbon material density and was in the range of 5 – 10 mg. The electrodes were tested in the two-electrode Swagelok® systems using stainless steel current collectors (316 L grade). The separator used was a single Whatman GF/A separator of 250 μm of uncompressed thickness. The electrolyte was 1 mol L^{-1} Li_2SO_4. For some experiments the reference electrode (Hg/Hg_2SO_4 in 0.5 mol L^{-1} K_2SO_4) was used to monitor the behaviour of individual electrodes according to the method presented elsewhere [43]. The electrochemical measurements were carried out on multichannel VMP potentiostat-galvanostat with EC-Lab software from BioLogic® (France). The techniques used in the research include cyclic voltammetry (1 – 50 mV s^{-1}), galvanostatic charging/discharging (0.1 – 10 A g^{-1}), leakage current measurements during potentiostatic hold (2 h) and self-discharge measurements (open circuit conditions for 12 h). The long-term stability of tested electrochemical capacitor system was evaluated using potentiostatic *floating* technique [44–46]. Each *floating* cycle consisted of three charging/discharging steps with a current load of 1 A g^{-1} followed by a voltage hold (1.5 V) for 2 h. Additionally, during ageing test cyclic voltammograms with a scanning rate of 5 mV s^{-1} were recorded in order to observe qualitative changes of studied system.

4. Results and discussion

In salt templating synthesis of carbon, adenine is a nucleobase, which has a high nitrogen content and an aromatic structure. Furthermore,

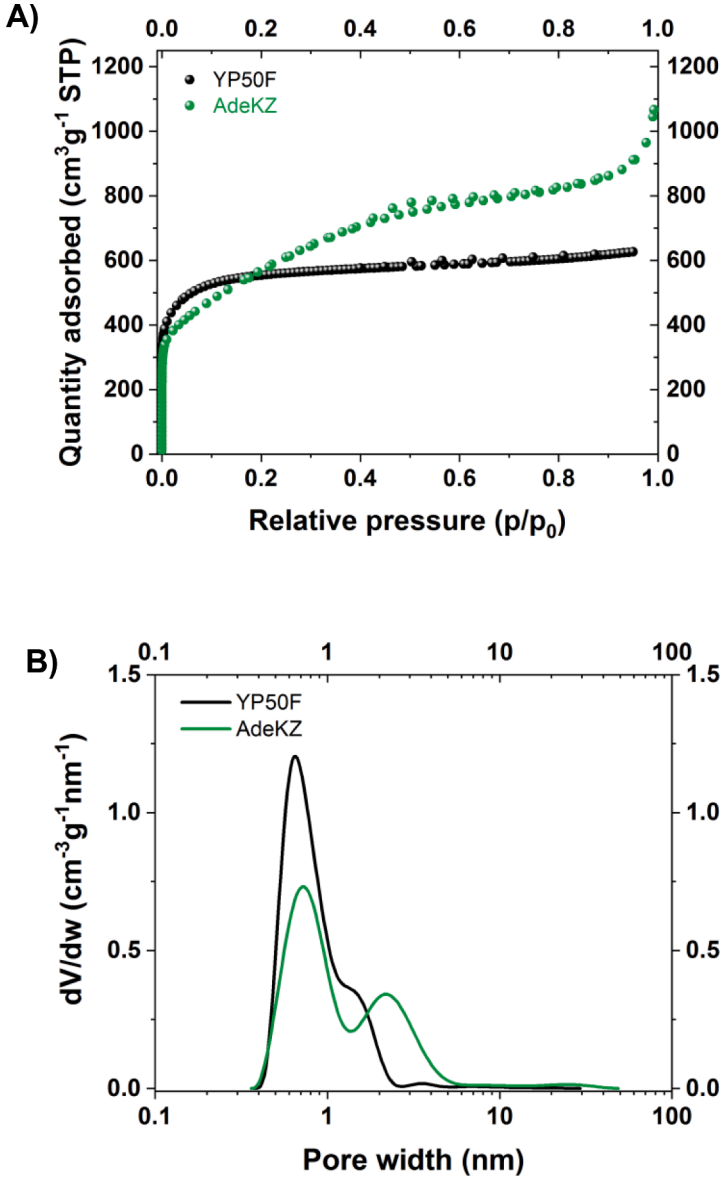

Fig. 1. Nitrogen adsorption measurements (77 K) of AdeKZ and YP50F carbon powders: **A)** adsorption/desorption isotherms; **B)** pore size distributions.

nucleobases are thermally stable. Pure adenine precursor is thermally relatively stable until 300 °C in inert gas. The adenine melting/decomposition starts at temperatures higher than 320 °C [39]. The melting/-decomposition temperature of adenine is higher comparing to the melting temperature (around 230 °C) [40] of the 1:1 mol.% $KCl/ZnCl_2$ inorganic mixture. This allows the solidification of the formed carbon in a homogenous salt melt phase. Additionally, the low melting point of the $KCl/ZnCl_2$ inorganic mixture favors the earlier salt phase mixing together with the crosslinking reactions of the carbon precursor and this leads to a micro and *meso* spherical carbon particle formation [40, 42]. This is supported by the SEM images of AdeKZ in Fig. S1, which shows a hierarchical pore structure with spherical like particles and interstitial pores in the *meso* to macropore range. Additionally, the 100 nm spherical carbon particles are interconnected. The larger spherical carbon particles are also composed of particle size beyond 100 nm, however, the SEM resolution is not sufficient to resolve this nanostructure. The XRD pattern (Fig. S2) shows typical diffraction peaks of an amorphous carbon at 22° and 44° for the (002) and (001), respectively. Furthermore, the XRD confirmed an almost complete removal of the salt template from the carbon structure.

In order to consider the real applicability of newly proposed material for electrochemical capacitor system, AdeKZ carbon was compared with the standard industrial carbon, i.e., Kuraray YP50F. Fig. 1 presents adsorption/desorption isotherm at 77 K for those two electrode materials. Both carbons are characterized by similar specific surface area, i.e., 1790 and 1760 $m^2\,g^{-1}$ for AdeKZ and YP50F, respectively. Nevertheless, as seen from Fig. 1B, their pore structure is considerably different. The isotherm of YP50F resembles typical microporous character of the material by exhibiting a sudden adsorption saturation even at low relative pressure. In case of AdeKZ, the adsorption increases slowly at 45° angle until $p/p_o = 0.4$, and then the plateau is reached. This adsorption curve shows the supermicropores abundance. Additionally, the mesopores presence is clearly indicated at p/p_o close to 1. Table 1 summarizes the values of adsorption data. The mesopore content is 9 times higher for AdeKZ than YP50F, while the micropore content is the same. It is visible that the total surface area is governed by micropores, while mesopores almost do not contribute to the specific surface area value.

The elemental composition has been determined using two techniques XPS and elemental analysis (EA) (Table 2). The total content of nitrogen from the entire sample volume for AdeKZ is equal to 5.5% as indicated by EA results. If this value is compared with the one given by XPS (4.1%) some discrepancy is found. As the XPS shows the composition within maximum few atomic layers inside the structure, it might be said that it reflects the surface composition. It can be therefore stated, that part of nitrogen is in the bulk of the sample rather than on the surface what can directly come from adenine structure as the precursor. Additionally, XPS data do not take into account H atomic% but detects traces of the templating agent, for instance, Zn (0.15%) and Cl (0.39%) as shown in Table S1. After deconvolution of N1s peak (Fig. 2), three components are identified for AdeKZ. It is revealed that mostly surface groups consist in quaternary type (401.0 eV, 54.9%), pyridinic (398.3 eV, 28.9%) and in much less concentration pyrrolic one (399.5 eV, 16.2%) [47]. The presence of pyridine, pyrrole and quaternary N enhances the capacitance of the system with N-rich carbon. Pyrrolic and pyridinic N contribute to the pseudocapacitance due to their e^- donor behaviour while the positive charge of quaternary N improves the electron transfer [18,19,30,31]. For comparison nitrogen was also analysed for YP50F carbon. This element was not found by EA analysis.

Table 1
The values from nitrogen adsorption/desorption experiment – specific surface area, total micro- and mesopore volumes.

Carbon	S_{BET} [$m^2\,g^{-1}$]	V_{micro} [$cm^3\,g^{-1}$]	V_{meso} [$cm^3\,g^{-1}$]
Ade KZ	1790	0.60	0.90
YP50F	1760	0.60	0.10

Some traces of N were detected by XPS (0.5% N). Furthermore, O1s peak deconvolution of AdeKZ (Figure S3 and Table S2) confirms the presence of C = O (530.6 eV, 17.2%), -COOH (531.5 eV, 5.8%) and OH (532.2 eV, 77.0%) surface groups as well as for YP50F, C = O (531.4 eV, 21.1%), -COOH (532.3 eV, 10.1%) and OH (533.5 eV, 68.8%) [48,49]. Presence of quinone, carboxyl and hydroxyl groups can contribute to the capacitance of the material through different redox reactions, by enhancing the EDL formation or by improving the wettability of the material [32–36]. When the total oxygen content is considered for AdeKZ, it is higher in the bulk (8.6%) than on the surface (2.4%). The opposite trend is obtained for YP50F carbon suggesting that most of oxygen comes from surface functionalities. It is worth highlighting that AdeKZ carbon contains relatively high amount of oxygen. Therefore, it is important to analyse carefully system lifetime since usually oxygen-rich carbons cause faster ECs degradation [18]. Due to a high concentration of oxygen the content of carbon is only 84%. Nevertheless, to sum up, the elemental analysis result agrees with XPS data. It is worth adding that AdeKZ surface appears to be positively charged due to the presence of quaternary nitrogen as shown in Table S4. In order to prove surface functionalities by different technique, FTIR spectra were recorded. Nitrogen signals around 3300 and 1550 cm^{-1} can be distinguished. This 1550 cm^{-1} signal (probably overlapped with C = C signal) is more intense for AdeKZ which correlates with the great amount of N present in this carbon. Additionally, N—H at 3300 cm^{-1} signal is only detected for the AdeKZ sample. C = O and C—O signals are shifted when comparing AdeKZ and YP50F probably due to their different environments (Figure S4). YP50F negative potential correlates with the high amount of oxygen groups observed by XPS. Moreover, XRD patterns for amorphous carbons YP50F and AdeKZ show characteristic graphite planes, (002) and (100/101), with similar moderate crystallinity (Figure S2). Raman spectra reveal that the I_D/I_G ratio is similar for both carbons ($I_D/I_G = 1.17$ for AdeKZ and $I_D/I_G = 1.02$ for YP50F) suggesting a similar presence of defects in the two carbons (Fig. S5).

An important difference of the carbon morphology can be seen on TEM micrographs. At the high magnification (Fig. 3A-B), YP50F carbon shows slightly more disordered and dense structure of the graphene layers than AdeKZ. Additionally, the d spacing in the AdeKZ graphene interlayers is 3.6 ± 0.4 Å (Fig. S6 A and Table S3). On the other hand, as it was previously discussed the YP50F has denser packaging of the graphene interlayers which results in a d spacing of 3.5 ± 0.2 Å (Fig S6 B and Table S3). This difference in morphology could be already seen in the lower magnification micrographs (Fig. 3C-D and Fig. S7). Here, the YP50F powder particles are 1–3 μm large and non-agglomerated, while the AdeKZ powder consists of agglomerates of carbon black-like morphologie, with a single particle size in the agglomerate being of about 100–500 nm (Fig. 3C-D). The improved contact of the AdeKZ particles could be responsible for high conductivity of this activated carbon material. Indeed, the conductivity measurements of dry carbon electrode indicated the values of 8 and 4.3 mS cm^{-1} for AdeKZ and YP50F, respectively. On the other hand, the AdeKZ and YP50F electrode densities are equal to 0.23 and 0.56 g cm^{-3}. More than twice less density of AdeKZ emerges from the fact of substantial mesopore contribution, causing that the carbon particles contain more voids, and therefore are lighter.

In addition, AdeKZ and YP50F carbons are characterized by different particle size distribution (Fig. 4). YP50F shows very narrow particle size distribution from 1 – 40 μm, centred at 8 μm. In the case of AdeKZ the particle size distribution is much broader. It has its maximum at around 25 μm, therefore bigger grains constitute AdeKZ than YP50F. It also displays smaller particles fraction. This broader particle size distribution allows for better conductivity of electrode material. According to the TEM micrograph of AdeKZ in Fig. 3C, it turns out that the fraction of greater particles (10 – 100 μm) is constituted by the clusters of smaller carbon particles. In contrast to the carbon black these small particles are not microscopic graphite particles (low capacitance, high conductivity), but of activated carbon (high capacitance). Therefore, it is possible to

Table 2
Elemental composition of AdeKZ and YP50F obtained from XPS and elemental analysis.

Sample	XPS					EA				
	C	H	N	O	sum (%)	C	H	N	O	sum (%)
AdeKZ	92.9	0	4.1	2.4	99.4	84.0	1.2	5.5	8.6	99.3
YP50F	94.2	0	0.5	5.3	100	95.4	1.7	0	2.3	99.4

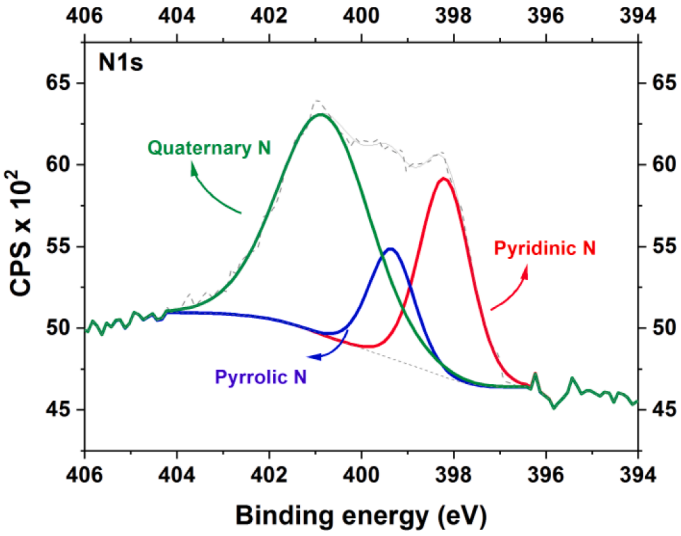

Fig. 2. XPS deconvolution of N1s region for AdeKZ.

benefit from high capacitance, while retaining high electrical conductivity.

The frequency response determined by electrochemical impedance spectroscopy of the symmetric AC/AC capacitors is shown in Fig. 5. Clearly, the use of micro/mesoporous AdeKZ provide better frequency response. Firstly, the capacitive response of AdeKZ rises faster with frequency decrease (100 kHz – 1 mHz) than for YP50F. The capacitance at 1 Hz is equal to 110 F g^{-1} and 42 F g^{-1} for AdeKZ and YP50F, respectively. Secondly, the final capacitance reached at low frequencies (average within the plateau) is 125 F g^{-1} and 100 F g^{-1} AdeKZ and YP50F, respectively. It is visible that in case of YP50F the low frequency capacitance indicates constant value, while in case of AdeKZ some small upward trend is observable. A slight increase of the capacitance is found at frequencies close to 1 mHz. It suggests the contribution of pseudo-capacitance, which can have the origin in high heteroatom (nitrogen, oxygen) content. The low-frequency capacitance measured for the symmetric cells indicates the capacitances of 105 and 133 F g^{-1} for YP50F and AdeKZ, respectively.

The extraordinary properties of AdeKZ carbon can be seen in the voltammetry experiment. The 1 mV s^{-1} voltammogram is perfectly rectangular showing only double-layer response. The increase of scan rate from 1 mV s^{-1} to 50 mV s^{-1} does not lead to the serious deterioration of the two-electrode voltammograms. This applies to the 1 V polarization (Fig. 6A). The situation is somewhat different when the maximum voltage was extended to 1.5 V (Fig. 6C). What is particularly seen at 1 mV s^{-1}, the redox reactions at the interface take place when the voltage exceeds about 1.3 V. Redox response diminishes as the scan rate is increased and still no signs of resistance are observable. Fig. 6B and D show the operation of the single electrodes in the capacitor. When the capacitor was polarized up to 1 V, perfectly rectangular voltammograms were obtained and no signs of redox reactions could be detected. The situation is different when the maximum voltage was extended to 1.5 V. Especially, the rapid current increase at the high potentials of positive electrode is visible. It comes from the electrode and/or electrolyte oxidation. Indeed, the electrode potential approaches the potential of equilibrium water decomposition. Oxygen or/and hydrogen evolution may be expected on the positive/negative side of the cell, respectively. According to the equation $E_0 = 1.23 - 0.059$ pH, the thermodynamic potential of oxygen evolution is 1.23 V at the pH of 0 and 0.81 V at pH of 7 (the initial pH of the electrolyte is neutral). From the voltammogram in Fig. 6D, a significant current increase is observed at 1.0 V vs. SHE. It could suggest that calculated pH at the positive electrode interface is therefore 3.9. The negative current hump during the reduction sweep at positive electrode reflects reduction of oxidized species formed during oxidation step. Negative electrode, on the other hand, does not show extensive reduction at low potentials that proves its better reversibility.

In order to verify the durability of AdeKZ based EC system in comparison to YP50F based one, long-term performance measurements were carried out. Accelerated ageing protocol, namely *floating* was performed for 200 h of potentiostatic hold at 1.5 V. As seen in Fig. 7A, the cycling of the AdeKZ capacitor is similar to the one of YP50F. The periodic fluctuations are of slight temperature variations. The relative capacitance is retained by 90% for AdeKZ, which is almost as high as in case of YP50F. However, this does not inform clearly about the changes occurred in the capacitor characteristics. Therefore, monitoring of the performance before and after 200 h floating test was done in the form of cyclic voltammograms. The results are shown in Fig. 7C and D for each system. It can be noticed that there are similar changes for both systems. Both characteristics are typical to the ageing in 1 mol L^{-1} Li_2SO_4 and several points can be discussed here [50]. First, the lower discharge capacitance is observed at the high voltage. This is a failure of positive electrode, which is progressively aggravated as the oxidation of electrode material leads to the production of gaseous CO_2 which escapes the interface. Also, the decreased current response at the end of charging is the effect of electrolyte acidification (owing to the as-produced CO_2 dissolution) or shift of the electrode potentials to less positive values. Second, a reversible current peak is appeared at about 0.6 V (quinone/hydroquinone redox response), and third, the current hump at the end of discharge (0.2 V – 0 V) appears. The third observation appears exclusively for YP50F. It corresponds to desorption of stored hydrogen at

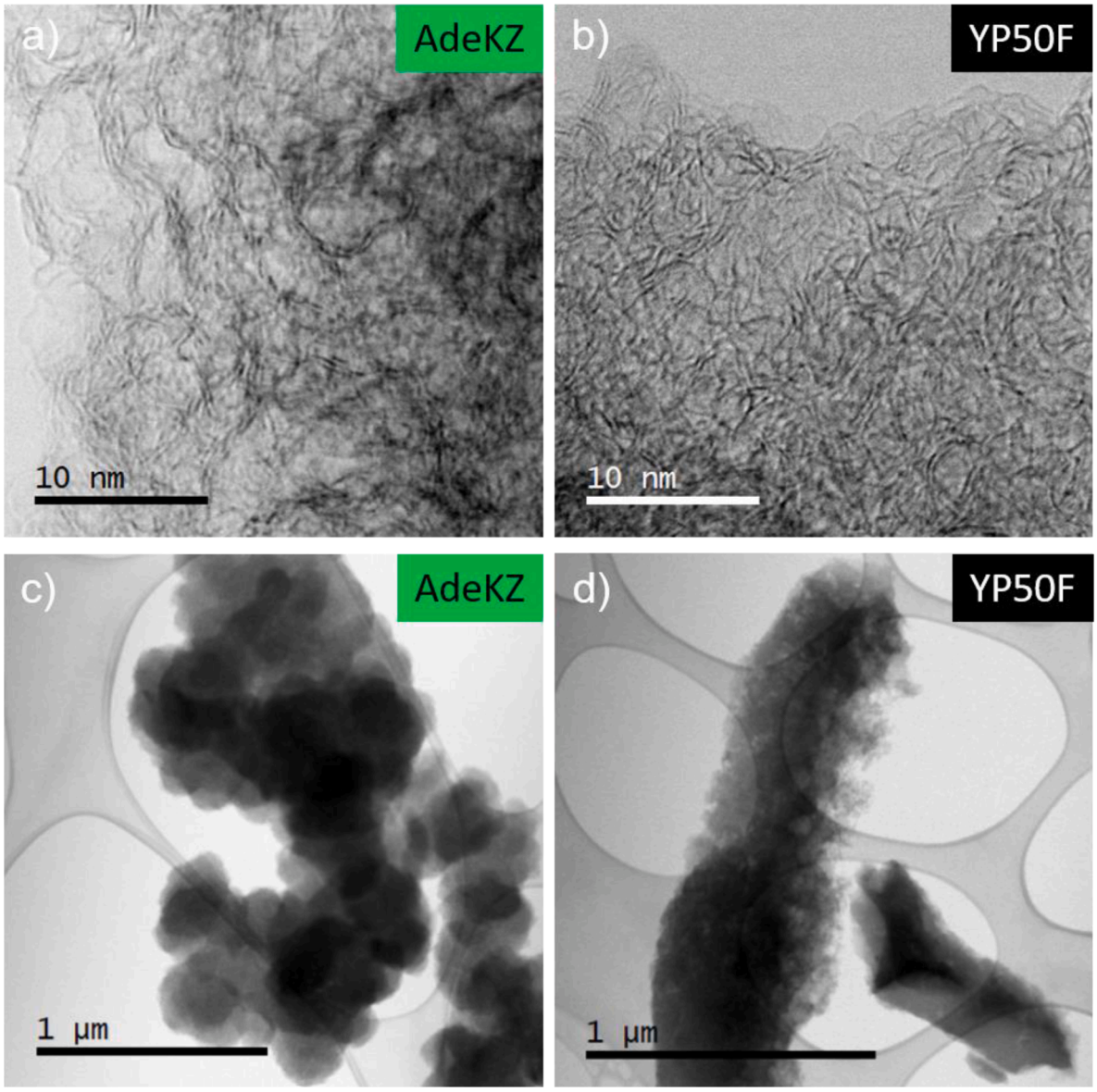

Fig. 3. STEM-BF images of: **A)** AdeKZ; **B)** YP50F high magnifications, showing structural differences and **C)** AdeKZ; **D)** YP50F at low magnification, showing the morphology differences.

negative electrode. It increases the coulombic efficiency but decreases the energetic one. Fig. 7B shows the specific surface area of the electrodes measured prior to and after cell disassembly. In comparison to the carbon powder, electrode surface is smaller (1460 vs. 1790 $m^2 g^{-1}$). This is an effect of binder addition to form the electrode from powder. The surface area for aged electrodes dropped both for negative (−20%) and positive electrode (−45%) for AdeKZ system. The drop in positive electrode is much more pronounced. This is, of course, due to the electrode material oxidation. The thorough analysis of textural properties, i.e. V_{micro} and V_{meso} indicate the drop after ageing process. As the positive electrode is being oxidized during the ageing process, its final V_{micro} drops almost twice in comparison to the fresh electrode (−41%). Its V_{meso} is affected to the similar degree (−36%). The main oxidation products are the oxygen containing functional groups on carbon as well as carbon dioxide. All these leads to the elimination of carbon graphitic edges and smoothing of porous texture. The negative electrode, on the other hand, is characterized especially by the decrease of V_{micro} rather than V_{meso}. This is related to the electrosorption of hydrogen, which occupies the active sites within the microporosity (Table S5).

To observe the surface groups changes after long-term capacitor operation, XPS analysis was carried out using aged electrodes both for AdeKZ as well as YP50F carbons. After capacitor cell disassembly, the individual electrodes were washed with distilled water to remove the residues of salt from electrolyte. Afterwards, they were dried and subjected to XPS analysis. Surface composition obtained from XPS data for all analysed samples is shown in Table S6. All the carbon electrodes in comparison to pure carbons (Table 2) contain fluorine owing to the PTFE binder. Various content of F on the surface of the electrode is the effect of binder distribution during electrode composite manufacturing. The silicon presence can be originated from separator (glassy fibre Whatman GF/A) which has been in direct contact with electrode surface. In the table, one may observe that oxygen content increased for each carbon after the ageing process for positive and negative electrodes. However, the increase of oxygen content is more visible for positive electrodes than in negative ones. For instance, in case of AdeKZ the amount of oxygen is almost doubled for positive electrode (8.5% vs. 17.5%). This perfectly fits the porosity measurements data obtained by N_2 sorption at 77 K. As proven in our previous research, this result can come from surface groups formation after long-term tests as well as insoluble solid state deposit (Li_2CO_3) precipitation. Since the negative

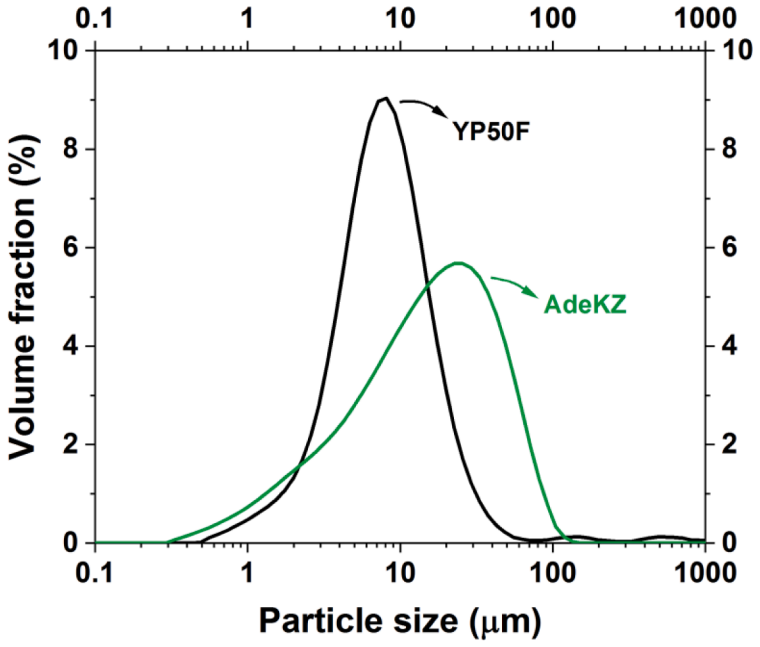

Fig. 4. Particle size distribution of AdeKZ (green) and YP50F (black).

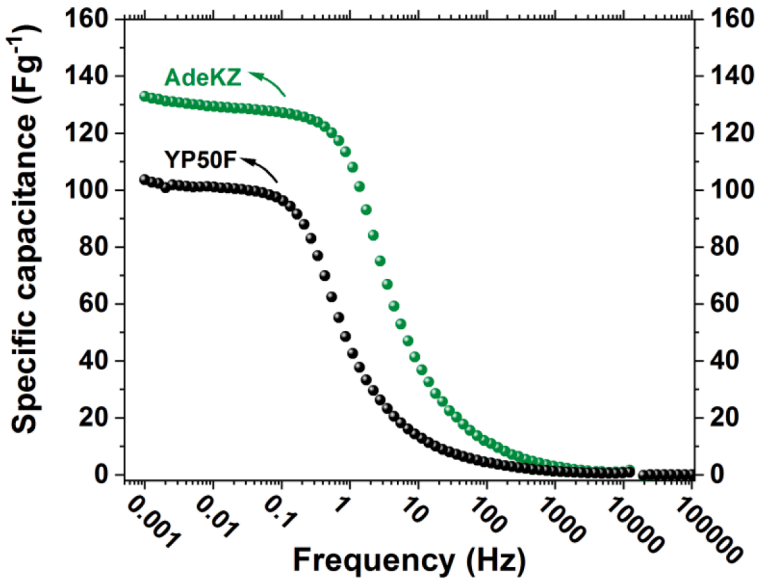

Fig. 5. Electrochemical impedance spectra (capacitance vs. frequency) recorded at 0 V for the AC/AC capacitors: YP50F (black), AdeKZ (green) in 1 mol L^{-1} Li_2SO_4.

electrode in electrochemical capacitor is not exposed to excessive oxidation at high potentials, it can be assumed that the slight oxygen increase (from 8.5% to 9.1% for AdeKZ and 7.1% to 9.3% for YP50F) can originate from Li_2CO_3. Fig. 8 shows the XPS spectra of oxygen (O1s) in AdeKZ electrode before and after the floating test (for positive and negative electrode separately).

The oxygen surface functionalities remain unchanged if the negative electrode is compared to the fresh one. The difference is observable if the positive electrode is compared with the fresh one. A tremendous increase of O—C bond is found confirming oxidation of the electrode. The difference between YP50F and AdeKZ carbons is noticed when the nitrogen content is considered. No nitrogen is detected for YP50F (which is correct), while in case of AdeKZ we might see some increase for both positive and negative electrodes after lifespan test. The increased value of nitrogen can be due to consumption of carbon, which will naturally increase the remaining elements content.

The analysis of carbon material capacitance and carbon material density led to the discussion on practical application of AdeKZ carbon in stationary and mobile energy storage systems (ESS). It is generally accepted that the mass of the system is not crucial in stationary applications. In case of mobile applications both volumetric and gravimetric capacitance is a matter, with the special emphasis on volumetric capacitance as the space for the ESS in the vehicles is strongly limited. Table 3 shows the comparative analysis of AdeKZ and YP50F where the capacitance values are expressed both in F g^{-1} and F cm^{-3}. Two scenarios should be distinguished for a complete analysis, as the performance of the capacitor is strongly correlated to the current regime of charging and discharging (which can be related with frequency). It was deduced on the experience that the frequency of 1 Hz corresponds to 10 A g^{-1} charging or discharging current regime. Namely, it is seen that in low frequency domain AdeKZ shows higher gravimetric capacitance than YP50F. At the same time, the volumetric capacitance is lower.

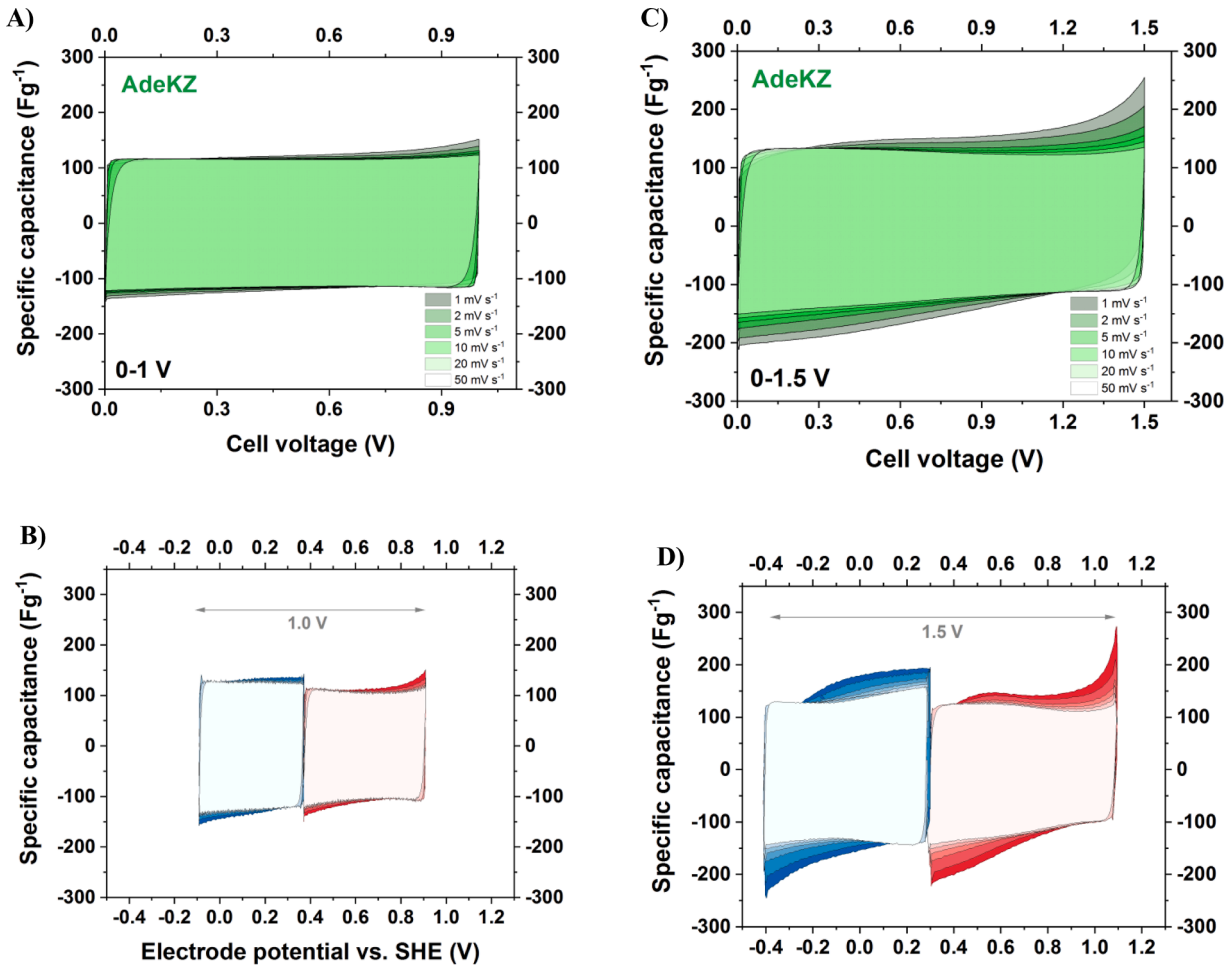

Fig. 6. Cyclic voltammograms (1 – 50 mV s^{-1}) of the AdeKZ-based capacitor in 1 mol L^{-1} Li_2SO_4: **A)** two-electrode voltammograms (0 - 1 V); **B)** voltammograms of single electrodes (0 - 1 V); **C)** two-electrode voltammograms (0 – 1.5 V); **D)** voltammograms of single electrodes (0 – 1.5 V).

Different situation is observed at high frequencies, where the gravimetric capacitance of AdeKZ is over twice higher than that of YP50F, where volumetric capacitance is comparable for both carbons. Taking into account that the capacitors are the devices which are intended to operate at high power, AdeKZ is superior to YP50F.

5. Conclusions

The results presented in the paper show the preparation, physicochemical and electrochemical analyses of the activated carbon produced from adenine precursor. The adenine carbon exhibits the substantial differences in comparison to commercial carbon (YP50F, Kuraray). Namely, although the total surface area of the carbons is comparable (1790 m^2 g^{-1} – AdeKZ and 1760 m^2 g^{-1} – YP50F), the gravimetric capacitance is 25% higher for adenine-based system. The difference is assigned to the supermicropores which turn out to be particularly useful. Another parameter which contributes to the increased capacitance is the nitrogen content of 5.5% (especially this of quaternary nature which exists in majority), which boosts the pseudocapacitance as well as the outstanding frequency response of the carbon. The high frequency response while retaining high capacitance is also enabled by the beneficial particle size distribution. It is composed of small particles that form clusters and resemble the morphology of high conductivity carbon black. Moreover, the voltammograms for tested cells do not show the resistive character until the scan rate of 50 mV s^{-1} what is a significant benefit of AdeKZ carbon. It was also proved that the system can operate at 1.5 V with practically no capacitance loss. The long-term performance of Ade-KZ was confirmed via floating technique which showed that the ageing process is typical of an activated carbon electrode operating in aqueous electrolyte of Li_2SO_4. The advantage of this carbon can be found by comparing its gravimetric and volumetric capacitance, that it is especially valuable in applications requiring high power (1 Hz or 10 A g^{-1}). In these conditions, AdeKZ system exhibits twice higher gravimetric capacitance than YP50F. Finally, it can be stated that adenine-based carbon is a good candidate for an electrochemical capacitor material, especially in high-power stationary application, where volume is not an issue. This statement is concluded based on a lab-scale device. It should be kept in mind that the real applicative aspects upon up-scaling can be precisely commented only if tested in actual conditions.

CRediT authorship contribution statement

Justyna Piwek: Conceptualization, Investigation, Writing – original draft, Data curation, Methodology. **Adam Slesinski:** Conceptualization, Writing – original draft, Data curation, Methodology. **Krzysztof Fic:** Formal analysis, Supervision. **Sergio Aina:** Investigation, Data curation. **Alen Vizintin:** Investigation, Writing – original draft. **Blaz Tratnik:** Investigation, Writing – original draft. **Elena Tchernychova:** Investigation. **Maria Pilar Lobera:** Investigation. **Maria Bernechea:** Funding acquisition, Supervision. **Robert Dominko:** Funding acquisition, Supervision. **Elzbieta Frackowiak:** Writing – review & editing, Supervision, Funding acquisition.

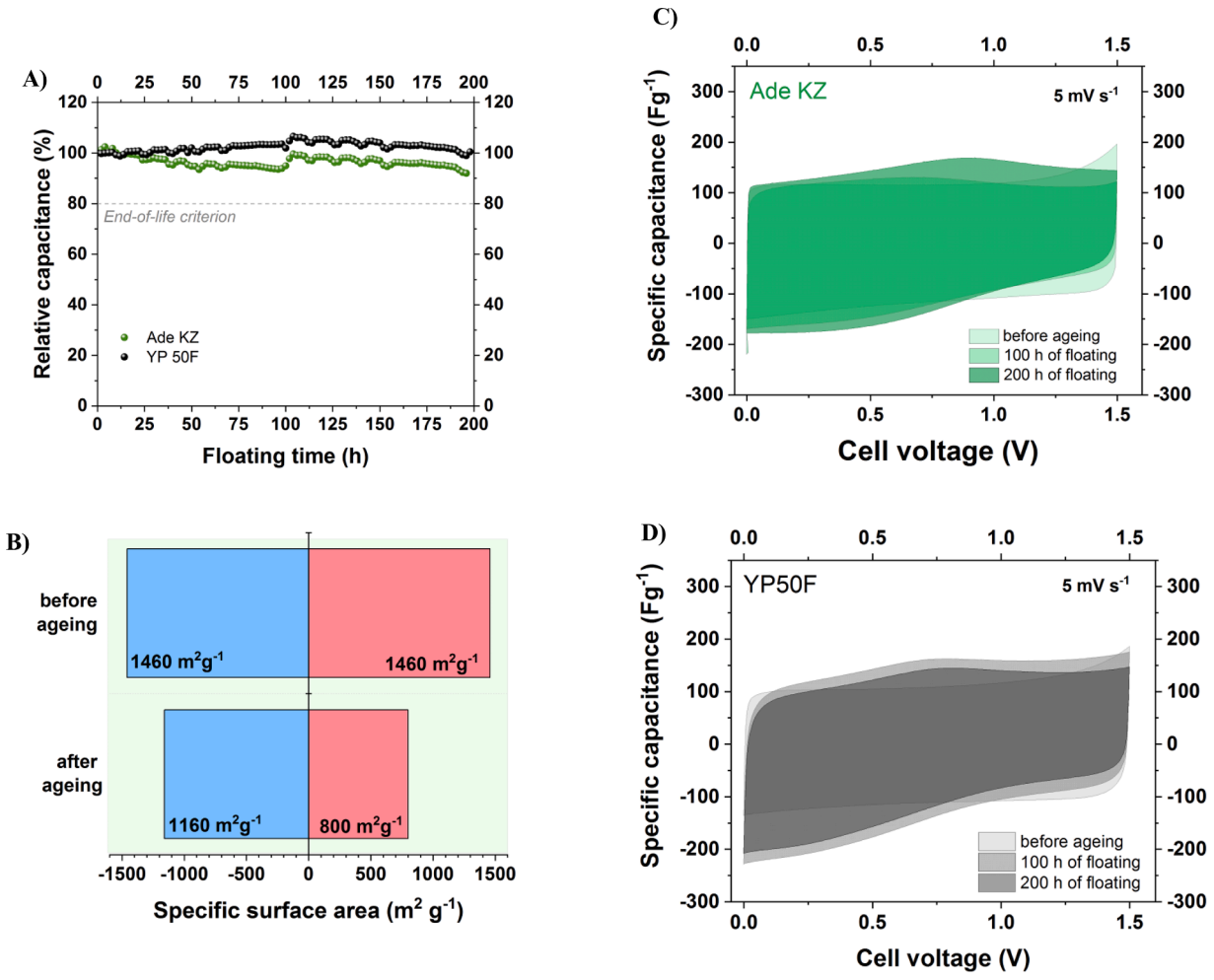

Fig. 7. Long term ageing test of AdeKZ and YP50F in 1 mol L^{-1} Li_2SO_4 at 1.5 V: **A)** capacitance retention in time; **B)** changes of electrodes' surface area for AdeKZ; **C)** CV (5 mV s^{-1}) before and after the floating for AdeKZ; **D)** CV (5 mV s^{-1}) before and after the floating for YP50F.

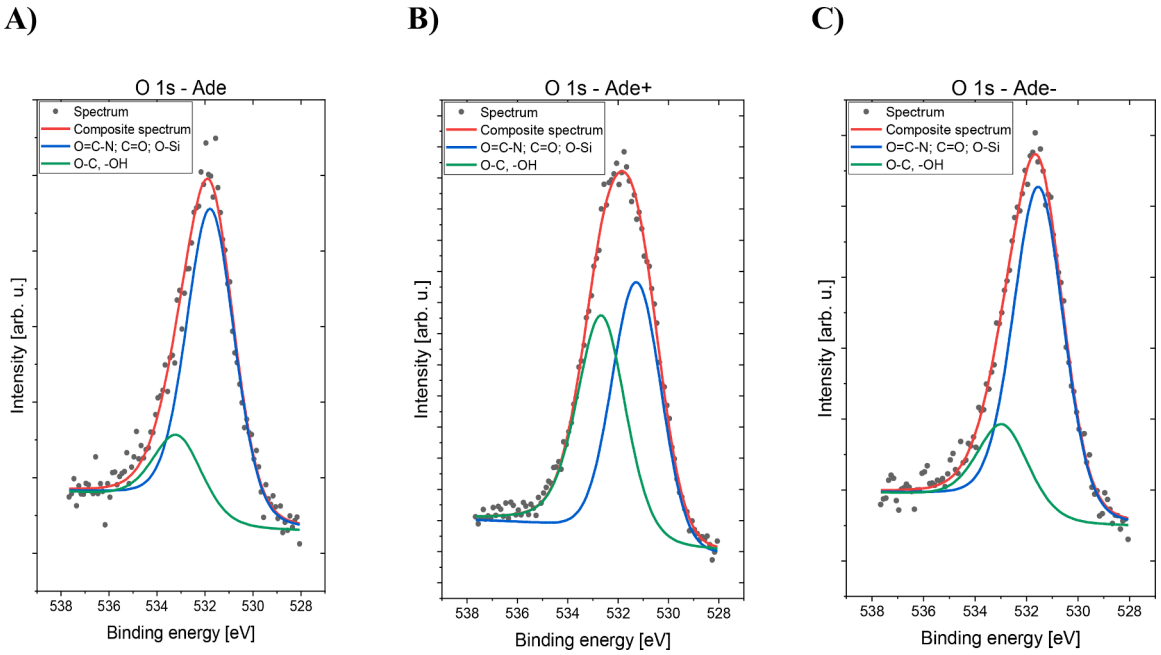

Fig. 8. XPS spectra of oxygen (O1s) in AdeKZ electrode: **A)** before the floating test, **B)** positive electrode after the floating test, **C)** negative electrode after the floating test.

Table 3
Gravimetric and volumetric dependencies of capacitance of AdeKZ carbon expressed on mass and volume bases.

Carbon electrode	Low frequency 1 mHz (~0.1 A g^{-1})		High frequency 1 Hz (~10 A g^{-1})	
	Gravimetric capacitance (F g^{-1})	Volumetric capacitance (F cm^{-3})	Gravimetric capacitance (F g^{-1})	Volumetric capacitance (F cm^{-3})
AdeKZ	125	29	107	25
YP50F	100	56	42	23

Declaration of Competing Interest

The authors declare that they have no known competing financial interests or personal relationships that could have appeared to influence the work reported in this paper.

Acknowledgement

Partners acknowledge M-ERA.NET network, MCIN/AEI/10.13039/501100011033 (Ref. PCI2019–103637), CIBER-BBN, ICTS "NANBIOSIS'', ICTS ELECMI node "Laboratorio de Microscopias Avanzadas", National Science Centre, Poland (2018/30/Z/ST4/00901), and Ministrstvo za izobraževanje, znanost in šport for financial support and the grant of Ministry of Science and Higher Education in Poland, no. 0911/SBAD/2101. A.V., B.T., E.T. and R.D. additionally acknowledge financial support from the Slovenian Research Agency (ARRS) research core funding P2–0393.

Supplementary materials

Supplementary material associated with this article can be found, in the online version, at doi:10.1016/j.electacta.2022.140649.

References

[1] M. Winter, R.J. Brodd, What are batteries, fuel cells, and supercapacitors? Chem. Rev. 104 (10) (2004) 4245.
[2] R. Kötz, M. Carlen, Principles and applications of electrochemical capacitors, Electrochim. Acta 45 (15) (2000) 2483–2498.
[3] P. Simon, Y. Gogotsi, Materials for electrochemical capacitors, Nat. Mater. 7 (11) (2008) 845.
[4] E. Frackowiak, Carbon materials for supercapacitor application, Phys. Chem. Chem. Phys. 9 (15) (2007) 1774–1785.
[5] F. Béguin, V. Presser, A. Balducci, E. Frackowiak, Carbons and electrolytes for advanced supercapacitors, Adv. Mater. 26 (14) (2014) 2219–2251.
[6] A. Krause, A. Balducci, High voltage electrochemical double layer capacitor containing mixtures of ionic liquids and organic carbonate as electrolytes, Electrochem. Commun. 13 (8) (2011) 814–817.
[7] A. Laheäär, P. Przygocki, Q. Abbas, F. Béguin, Appropriate methods for evaluating the efficiency and capacitive behavior of different types of supercapacitors, Electrochem. Commun. 60 (2015) 21–25.
[8] B. Lobato, L. Suárez, L. Guardia, T.A. Centeno, Capacitance and surface of carbons in supercapacitors, Carbon (New York) 122 (2017) 434–445.
[9] R. Kötz, M. Hahn, R. Gallay, Temperature behavior and impedance fundamentals of supercapacitors, J. Power Sources 154 (2) (2006) 550–555.
[10] L. Suárez, V. Barranco, T.A. Centeno, Impact of carbon pores size on ionic liquid based-supercapacitor performance, J. Colloid Interface Sci 588 (2021) 705–712.
[11] P. Simon, Y. Gogotsi, Capacitive energy storage in nanostructured carbon–electrolyte systems, Acc. Chem. Res. 46 (5) (2013) 1094–1103.
[12] G. Gryglewicz, J. Machnikowski, E. Lorenc-Grabowska, G. Lota, E. Frackowiak, Effect of pore size distribution of coal-based activated carbons on double layer capacitance, Electrochim. Acta 50 (5) (2005) 1197–1206.
[13] K. Fic, E. Frackowiak, F. Béguin, Unusual energy enhancement in carbon-based electrochemical capacitors, J. Mater. Chem. 22 (46) (2012) 24213.
[14] J. Menzel, K. Fic, M. Meller, E. Frackowiak, The effect of halide ion concentration on capacitor performance, J. Appl. Electrochem. 44 (4) (2014) 439–445.
[15] M. Meller, K. Fic, J. Menzel, E. Frackowiak, Electrode/electrolyte interface with various redox couples, ECS Trans. 61 (14) (2014) 1–8.
[16] B. Gorska, P. Bujewska, K. Fic, Thiocyanates as attractive redox-active electrolytes for high-energy and environmentally-friendly electrochemical capacitors, Phys. Chem. Chem. Phys. 19 (11) (2017) 7923–7935.
[17] D. Salinas-Torres, S. Shiraishi, E. Morallón, D. Cazorla-Amorós, Improvement of carbon materials performance by nitrogen functional groups in electrochemical capacitors in organic electrolyte at severe conditions, Carbon (New York) 82 (2015) 205–213.
[18] D. Hulicova-Jurcakova, M. Seredych, G.Q. Lu, T.J. Bandosz, Combined effect of nitrogen- and oxygen-containing functional groups of microporous activated carbon on its electrochemical performance in supercapacitors, Adv. Funct. Mater. 19 (3) (2009) 438–447.
[19] B. Li, F. Dai, Q. Xiao, L. Yang, J. Shen, C. Zhang, M. Cai, Nitrogen-doped activated carbon for a high energy hybrid supercapacitor, Energy Environ. Sci. 9 (1) (2016) 102–106.
[20] C.-.T. Hsieh, H. Teng, Influence of oxygen treatment on electric double-layer capacitance of activated carbon fabrics, Carbon (New York) 40 (5) (2002) 667–674.
[21] Y.-.R. Nian, T. Hsisheng, Nitric acid modification of activated carbon electrodes for improvement of electrochemical capacitance, J. Electrochem. Soc. 149 (8) (2002) A1008–A1014.
[22] C.-.C. Hu, C.-.C. Wang, Effects of electrolytes and electrochemical pretreatments on the capacitive characteristics of activated carbon fabrics for supercapacitors, J. Power Sources 125 (2) (2004) 299–308.
[23] A. Slesinski, C. Matei-Ghimbeu, K. Fic, F. Béguin, E. Frackowiak, Self-buffered pH at carbon surfaces in aqueous supercapacitors, Carbon N Y 129 (2018) 758–765.
[24] H. Marsh, F. Rodriguez-Reinoso, Activated Carbon, Elsevier Science & Technology, Oxford, 2006. Oxford.
[25] G. Pognon, T. Brousse, D. Bélanger, Effect of molecular grafting on the pore size distribution and the double layer capacitance of activated carbon for electrochemical double layer capacitors, Carbon (New York) 49 (4) (2011) 1340–1348.
[26] J. Yan, T. Wei, Z. Fan, W. Qian, M. Zhang, X. Shen, F. Wei, Preparation of graphene nanosheet/carbon nanotube/polyaniline composite as electrode material for supercapacitors, J. Power Sources 195 (9) (2010) 3041–3045.
[27] G. Shul, D. Bélanger, Self-discharge of electrochemical capacitors based on soluble or grafted quinone, Phys. Chem. Chem. Phys. 18 (28) (2016) 19137–19145.
[28] M. Seredych, D. Hulicova-Jurcakova, G.Q. Lu, T.J. Bandosz, Surface functional groups of carbons and the effects of their chemical character, density and accessibility to ions on electrochemical performance, Carbon (New York) 46 (11) (2008) 1475–1488.
[29] K. Malaie, M.R. Ganjali, F. Soavi, Toward low-cost and sustainable supercapacitor electrode processing: simultaneous carbon grafting and coating of mixed-valence metal oxides by fast annealing, Front. Chem. 7 (2019), 25-25.
[30] I.M. Rocha, O.S.G.P. Soares, D.M. Fernandes, C. Freire, J.L. Figueiredo, M.F. R. Pereira, N-doped carbon nanotubes for the oxygen reduction reaction in alkaline medium: synergistic relationship between pyridinic and quaternary nitrogen, ChemistrySelect (Weinheim) 1 (10) (2016) 2522–2530.
[31] M. Yang, B. Cheng, H. Song, X. Chen, Preparation and electrochemical performance of polyaniline-based carbon nanotubes as electrode material for supercapacitor, Electrochim. Acta 55 (23) (2010) 7021–7027.
[32] X. Feng, Y. Bai, M. Liu, Y. Li, H. Yang, X. Wang, C. Wu, Untangling the respective effects of heteroatom-doped carbon materials in batteries, supercapacitors and the ORR to design high performance materials, Energy Environ. Sci. 14 (4) (2021) 236–289.
[33] K. Okajima, K. Ohta, M. Sudoh, Capacitance behavior of activated carbon fibers with oxygen-plasma treatment, Electrochim. Acta 50 (11) (2005) 2227–2231.
[34] H. Oda, A. Yamashita, S. Minoura, M. Okamoto, T. Morimoto, Modification of the oxygen-containing functional group on activated carbon fiber in electrodes of an electric double-layer capacitor, J. Power Sources 158 (2) (2006) 1510–1516.
[35] M.-.A. Goulet, M. Skyllas-Kazacos, E. Kjeang, The importance of wetting in carbon paper electrodes for vanadium redox reactions, Carbon (New York) 101 (2016) 390–398.
[36] G. Zhou, C. Xu, W. Cheng, Q. Zhang, W. Nie, Effects of oxygen element and oxygen-containing functional groups on surface wettability of coal dust with various metamorphic degrees based on XPS experiment, J. Anal. Methods Chem. 2015 (2015) 467242–467248.
[37] S. Kubo, R. Demir-Cakan, L. Zhao, R.J. White, M.-.M. Titirici, Porous Carbohydrate-Based Materials via Hard Templating, ChemSusChem 3 (2) (2010) 188–194.
[38] L. Chuenchom, R. Kraehnert, B.M. Smarsly, Recent progress in soft-templating of porous carbon materials, Soft. Matter. 8 (42) (2012) 181–1812.
[39] J. Pampel, A. Mehmood, M. Antonietti, T.-.P. Fellinger, Ionothermal template transformations for preparation of tubular porous nitrogen doped carbons, Mater. Horiz. 4 (3) (2017) 493.
[40] J. Pampel, C. Denton, T.-.P. Fellinger, Glucose derived ionothermal carbons with tailor-made porosity, Carbon (New York) 107 (2016) 288–296.
[41] F. Schipper, A. Vizintin, J. Ren, R. Dominko, T.-.P. Fellinger, Biomass-derived heteroatom-doped carbon aerogels from a salt melt sol-gel synthesis and their performance in Li-S batteries, ChemSusChem 8 (18) (2015) 3077–3083.
[42] N. Fechler, T.-.P. Fellinger, M. Antonietti, Salt templating": a simple and sustainable pathway toward highly porous functional carbons from ionic liquids, Adv. Mater. (Weinheim) 25 (1) (2013) 75–79.
[43] A. Slesinski, E. Frackowiak, Determination of accurate electrode contribution during voltammetry scan of electrochemical capacitors, J. Solid State Electrochem. 22 (7) (2018) 2135–2139.
[44] D. Weingarth, A. Foelske-Schmitz, R. Kötz, Cycle versus voltage hold – Which is the better stability test for electrochemical double layer capacitors? J. Power Sources 225 (2013) 84–88.
[45] J. Piwek, A. Platek, E. Frackowiak, K. Fic, Mechanisms of the performance fading of carbon-based electrochemical capacitors operating in a LiNO3 electrolyte, J. Power Sources 438 (2019).

[46] R. German, A. Sari, P. Venet, Y. Zitouni, O. Briat, J.-.M. Vinassa, Ageing Law For Supercapacitors Floating Ageing, IEEE, 2014, pp. 1773–1777.
[47] D. Sebastián, M. Nieto-Monge, S. Pérez-Rodríguez, E. Pastor, M. Lázaro, Nitrogen doped ordered mesoporous carbon as support of PtRu nanoparticles for methanol electro-oxidation, Energies (Basel) 11 (4) (2018) 831.
[48] G. Lan, Y. Qiu, J. Fan, X. Wang, H. Tang, W. Han, H. Liu, H. Liu, S. Song, Y. Li, Defective graphene@diamond hybrid nanocarbon material as an effective and stable metal-free catalyst for acetylene hydrochlorination, Chem. Commun. (Camb.) 55 (10) (2019) 1430–1433.
[49] Y.C.G. Kwan, G.M. Ng, C.H.A. Huan, Identification of functional groups and determination of carboxyl formation temperature in graphene oxide using the XPS O 1 s spectrum, Thin Solid Films 590 (2015) 40–48.
[50] K. Fic, A. Platek, J. Piwek, J. Menzel, A. Ślesiński, P. Bujewska, P. Galek, E. Frąckowiak, Revisited insights into charge storage mechanisms in electrochemical capacitors with Li2SO4-based electrolyte, Energy Storage Mater. 22 (2019) 1–14.